Proc. Natl. Acad. Sci. USA
Vol. 96, pp. 6014–6019, May 1999
Chemistry

Femtosecond dynamics of DNA-mediated electron transfer

CHAOZHI WAN, TORSTEN FIEBIG, SHANA O. KELLEY, CHRISTOPHER R. TREADWAY, JACQUELINE K. BARTON†, AND AHMED H. ZEWAIL†

Laboratory for Molecular Sciences, Arthur Amos Noyes Laboratory of Chemical Physics, California Institute of Technology, Pasadena, CA 91125

Contributed by Ahmed H. Zewail, March 26, 1999

ABSTRACT **Diverse biophysical and biochemical studies have sought to understand electron transfer (ET) in DNA in part because of its importance to DNA damage and its repair. However, the dynamics and mechanisms of the elementary processes of ET in this medium are not fully understood and have been heavily debated. Two fundamental issues are the distance over which charge is transported and the time-scale on which the transport through the π-stack of the DNA base pairs may occur. With femtosecond resolution, we report direct observation in DNA of ultrafast ET, initiated by excitation of tethered ethidium (E), the intercalated electron acceptor (A); the electron donor (D) is 7-deazaguanine (Z), a modified base, placed at different, fixed distances from A. The ultrafast ET between these reactants in DNA has been observed with time constants of 5 ps and 75 ps and was found to be essentially independent of the D–A separation (10–17 Å). However, the ET efficiency does depend on the D–A distance. The 5-ps decay corresponds to direct ET observed from 7-deazaguanine but not guanine to E. From measurements of orientation anisotropies, we conclude that the slower 75-ps process requires the reorientation of E before ET, similar to E/nucleotide complexes in water. These results reveal the nature of ultrafast ET and its mechanism: in DNA, ET cannot be described as in proteins simply by a phenomenological parameter, β. Instead, the involvement of the base pairs controls the time scale and the degree of coherent transport.**

The striking resemblance of the base-pair stack of DNA to conductive one-dimensional aromatic crystals prompted, over 30 years ago, the proposal that long-range charge transport might proceed through DNA (1). In the three decades since, biochemical, biophysical, and theoretical studies have sought to address the possibility and efficiency of the transport (2–29). Such charge migration through DNA is significant, because radical migration is a critical issue to our understanding of carcinogenesis and mutagenesis (5, 6).

Photoinduced electron transfer (ET) reactions have provided a useful tool in elucidating parameters governing ET through DNA. In the 1980s and early 90s, a class of experiments on noncovalently bound electron donors (D) and electron acceptors (A) in DNA was reported (7–12). A major debate focused on whether or not ET through DNA may proceed rapidly and differently from that found in σ-bonded systems. These experiments provided valuable information and raised many questions, but a key issue was the distance between D and A, which was not well defined.

With D and A covalently bonded to DNA, studies of ET on more well defined assemblies were made possible, and the effect of distance could be addressed (13–20). Values of the parameter β, which reflects the distance scale of ET through a given medium (30), remarkably, ranged from ≤ 0.1 Å^{-1} to >1.4 Å^{-1}; β was estimated by using one system of a fixed distance (13, 14) or by varying the distance (15–20). The fact that values of β could vary so enormously created substantial controversy. Recently, studies of ET between modified bases in DNA (20) were reported with β spanning this full range depending on stacking of reactants (16). Long-range oxidative damage and repair to DNA have been reported for covalently bound oxidants (17, 27–29). Moreover, recent conductivity measurements have shown the existence of both dark and photoinduced one-dimensional currents along DNA that were aligned in flexible-cast DNA films (3). Theoretical efforts (21–26) have discussed the different modes of ET, direct tunneling vs. hopping, and the possible range of β for DNA; a prediction of β for DNA of 1.2–1.6 Å^{-1} was made (21). The importance of the β-value is in relating rates to the mechanism, an area that has received considerable attention in the studies of ET in proteins [refs. 31 (and references therein), 32, and 33].

The direct observation of the ultrafast dynamics of DNA-mediated ET is critical to our understanding of the mechanism. With femtosecond resolution, it is now possible to obtain the actual time scale of ET and to relate the rates to the distance between D and A. The time scale of orientational coherence and solvation can also be examined, allowing us to elucidate the role of molecular motions.

The DNA Assemblies

ET between ethidium (E) and 7-deazaguanine (Z) has been characterized previously in aqueous solution (34). By using femtosecond spectroscopy, ET was found to proceed between photoexcited E and associated Z triphosphate (ZTP) but not between E and the natural analogue GTP. The measured peak potential of the cyclovoltametry, which is taken as an estimate of the standard potential, is 1.0 V and 1.3 V (vs. normal hydrogen electrode) for $ZTP^{\bullet +}/ZTP$ and $GTP^{\bullet +}/GTP$, respectively; the peak potential for $E^{+*}/E^{\bullet}$ is 1.2 V (after subtracting the 0–0 excitation energy from the ground-state peak potential for $E^{+}/E^{\bullet}$) (18). The ET dynamics of the E/ZTP system were ultrafast but reflected the time required for the reorientation of the complex into an active conformation for charge transfer (34). The quenching of the E* fluorescence was studied in a DNA assembly as a function of distance and sequence (18). In Z-containing duplexes covalently modified with E, steady-state fluorescence measurements revealed a shallow dependence of the efficiency of the quenching on distance, but the reaction dynamics could not be resolved by picosecond single-photon counting.

Fig. 1*a* illustrates models of three DNA assemblies used in the studies reported here. In these 14-mer duplexes containing tethered E, the position of Z has been varied so as to give a range of D–A separations; the sequence representing the binding site for E and the sequence flanking Z have been kept constant. Fluorescence-decay profiles, steady-state fluores-

The publication costs of this article were defrayed in part by page charge payment. This article must therefore be hereby marked "*advertisement*" in accordance with 18 U.S.C. §1734 solely to indicate this fact.

PNAS is available online at www.pnas.org.

Abbreviations: ET, electron transfer; E, ethidium; A, electron acceptor; D, electron donor; Z, 7-deazaguanine; ZTP, Z triphosphate; G, guanine; B, bridge.

†To whom reprint requests should be addressed. e-mail: jkbarton@its.caltech.edu or zewail@cco.caltech.edu.

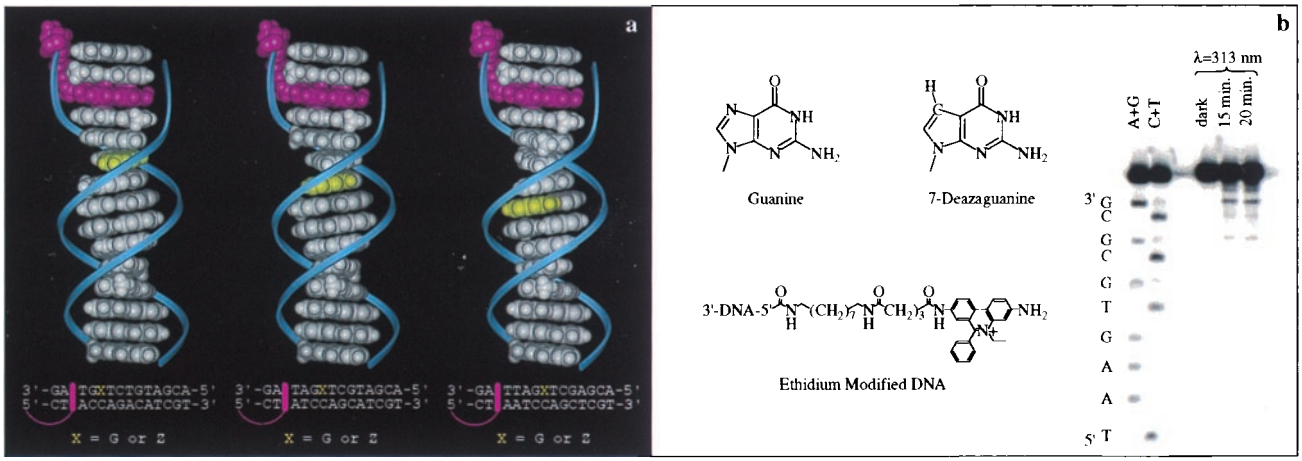

FIG. 1. The DNA assemblies. (*a*) Molecular models (Insight II) illustrating the E-tethered (red) DNA assemblies (left to right) 5Z, 6Z, and 7Z. The Z base is shown in yellow. Sequences are given below. (*b*) Structures of guanine (G), Z, and the E-modified tether, as well as an autoradiogram (right) after denaturing 18% PAGE, showing photoinduced damage of an E-modified duplex generated by irradiation at 313 nm of the duplex (10 μM) in 5 mM phosphate/50 mM NaCl, pH 7, 5′ ^{32}P-labeled on the strand complementary to that containing the tether. Crosslinking occurs at the first two base steps on the 3′ side (near E); see *The DNA Assemblies* and ref. 35. The sequence 3′-CGCGCACTTA-5′ also was examined and gave consistent results.

cence polarization measurements, thermal denaturation profiles, ionic-strength effects, and studies using various linker lengths all indicate that the tethered E moiety is intercalated within the DNA duplex. These data are also consistent with a homogeneous assembly in the steady-state regime (16, 18). Fig. 1*a* depicts E intercalated at the second base step of the assembly; molecular modeling indicates this second base step to be the farthest possible site from the end of the hybridized duplex into which the tethered E can intercalate, although the first base step is preferred.

To examine experimentally the distribution of binding sites for E within the tethered duplex, a series of photocrosslinking experiments were undertaken. Irradiation of E-modified duplexes at a short wavelength (313 nm) leads to covalent crosslinking at the site of intercalation and strange breakage; the resultant damage can be visualized by denaturing PAGE (35). Fig. 1*b* shows the damage on the strand complementary to that modified with E. Quantitation of gel bands indicates a narrow distribution of binding sites, with ≥70% of tethered E intercalated at the first base step and the remaining E bound predominantly within the second base step from the terminus. Here, then we consider, conservatively, tethered E as intercalated within the second base step, such that the intrahelix distance separating E and Z in the 5Z assembly is 10 Å (assuming 3.4-Å stacking); for 6Z and 7Z the distance is 14 Å and 17 Å, respectively.

ET Dynamics

To study the dynamics of ET in real time, we performed femtosecond transient absorption measurements on the molecular assemblies shown in Fig. 1. The detailed experimental setup has been described elsewhere (34). Briefly, a femtosecond pulse at 500 nm was employed to excite E into its excited state (S_1), and a second pulse at ≈400 nm, after a variable time delay, was used to probe the dynamics of this state. The dramatic differences in the transient absorption decays of 5G and 5Z can be seen in Fig. 2 *a* and *d*. In the short time range, 5G shows the expected lifetime of tethered E in DNA: ≈2-ns decay background with a small (14%) 1.5-ps decay component; the lifetime of E* functionalized on the exocyclic amine is ≈2 ns when tethered to DNA (16), compared with ≈20 ns for unfunctionalized E* in DNA (36, 37). In contrast, 5Z decays with a much stronger 5-ps component (34%); at longer times, the decay of 5Z shows a 75-ps (23%) component, which is absent in 5G, with the ≈2-ns decay (43%) present (Fig. 2*d*).

To ensure that the decay is that of the initial excited E population, we also performed femtosecond fluorescence up-conversion measurements. The fluorescence transients were detected in the wavelength range between 570 nm and 670 nm. Fig. 3 shows the transients of 5G and 5Z at 600 nm and 670 nm. As in the transient absorption, significant differences in the fluorescence transients of 5G and 5Z were observed. In the short time range (at 600 nm), the lifetime of E* (Fig. 3*a*) is shortened in 5Z ($\tau \approx 5$ ps); As with transient absorption, we can fit the early time decay to the same 1.5-ps component, but the signal-to-noise ratio for the fluorescence up-conversion is not as good as for transient absorption. At longer times and at 600 nm (Fig. 3*b*), the fluorescence decay of 5G consists predominantly of the ≈2-ns component (with a possible small 20-ps component), whereas 5Z shows a stronger decay with the expected time constant of ≈75 ps and the ≈2-ns decay. After the 5-ps and 75-ps decays, the fluorescence intensity of 5Z decreases significantly when compared with 5G; i.e., the ultrashort fluorescence lifetime component in 5Z reflects the onset of a major nonradiative process brought about by the D–B–A (B = bridge) of the DNA assembly.

The unambiguous presence of two distinguishable time scales for such processes in the assemblies containing Z raises the following question: Are the 5-ps and 75-ps decays caused by ET? As determined by electrochemical studies (18), ΔG for ET is ≈ -0.2 eV (E*/Z) and +0.1 eV (E*/G), respectively (note that 1 eV = 1.602×10^{-19} J). Hence, there is a favorable driving force for ET with Z but not with G. Energy transfer is not significant because of the lack of spectral overlap between D and A. Because Z and G differ by only one atom, other nonradiative processes can be excluded. We conclude that ET leads to the dynamics observed in the Z assemblies. It is important to note that both time constants observed (5 ps and 75 ps) reflect the *forward* ET dynamics, because the fluorescence intensity of the product radical state is supposed to be much weaker than that of the initial state, monitored in both the transient absorption and fluorescence up-conversion experiments.

For the same D–A system, without DNA mediation, it was found that solvation of E occurs on the time scale of femtoseconds and up to 1 ps in water; furthermore, the orientation time of E was measured to be ≈70 ps (34). To examine solvation and internal rotation when DNA is mediating the

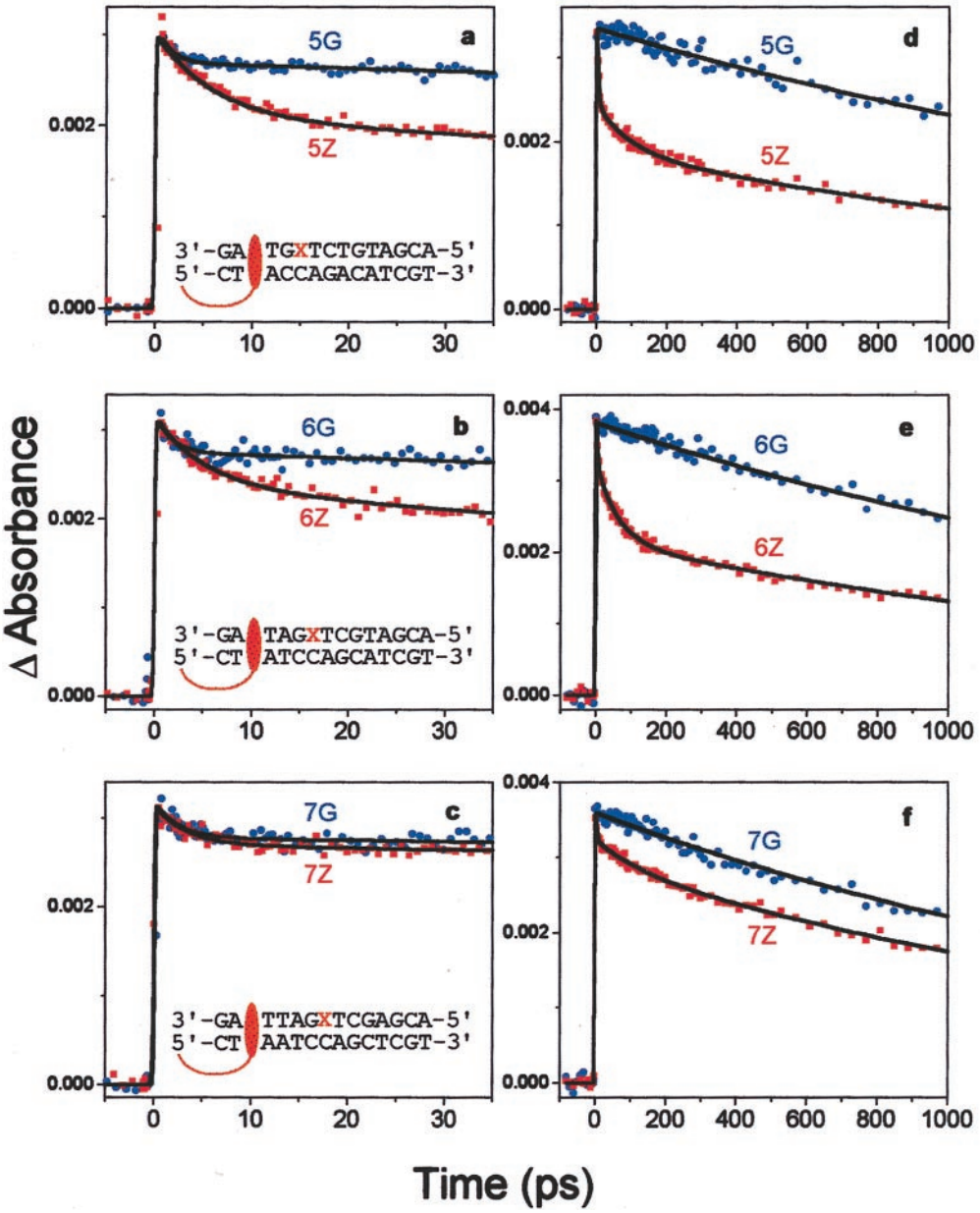

FIG. 2. Femtosecond transient absorption of DNA assemblies with 5Z/5G, 6Z/6G, and 7Z/7G after excitation at 500 nm (probed at 400 nm); short (*Left*) and long (*Right*) time scales are shown. All samples contained 10 μM duplex DNA in 5 mM phosphate/50 mM NaCl, pH 7. The sequences are displayed with closest position of E indicated.

transfer, we studied the wavelength dependence of the fluorescence transients and the time dependence of the fluorescence anisotropy. At the longer wavelength (670 nm; Fig. 3 *c* and *d*) the fluorescence signal of 5G rises, and we fitted this picosecond rise to 1.5-ps and 20-ps components (10–20%); the signal-to-noise is not sufficient to provide accurate values but the picosecond rise is definite. As shown in Fig. 3*b*, 5Z exhibits the same 75-ps decay component observed at 600 nm. The fact that the transient appears as a decay at the short wavelength and as a rise at the longer wavelength suggests that the ultrafast dynamics in 5G reflect a temporal spectral shift. Such a shift can be caused by solvation dynamics and/or structural relaxation processes; a 1.5-ps decay is consistent with the solvation process (34). The longer picosecond component may be attributed to structural relaxation, such as the phenyl-ring rotation (38), probed in fluorescence (not transient absorption) because of the sensitivity of fluorescence detection to a subset of molecular configurations. Naturally, the same processes are expected to be present in 5G and 5Z; however, the dominant 5-ps decay in 5Z almost cancels the picosecond rise components, which would be expected at 670 nm because of the spectral shift, hence the observed flattening in Fig. 3*c*.

To answer the question as to why there are two apparent time scales for ET (5 ps and 75 ps), we performed femtosecond fluorescence anisotropy measurements. The anisotropies $r(t)$ are derived from the intensity of the parallel $I_{\parallel}(t)$ and perpendicular $I_{\perp}(t)$ up-conversion signals by using the following formula: $r(t) = [I_{\parallel}(t) - I_{\perp}(t)]/[I_{\parallel}(t) + 2I_{\perp}(t)]$. Fig. 4 *a* and *c* shows the anisotropy of the 5G and 5Z assemblies. It is interesting that 5Z shows a single slow decay ($\approx$5 ns); 5G shows a similar decay but with an additional decay component ($\approx$12%) of $\approx$100 ps. The $\approx$100-ps and $\approx$5-ns anisotropy decays of 5G are ascribed to the restricted rotation of E in DNA and other slower rotations, including that of the whole DNA duplex (37, 39, 40). As discussed elsewhere (34), the fact that the $\approx$100-ps anisotropy decay exists in 5G but not in 5Z indicates that there is a correlation of the slow ET process (75 ps) with the rotation of E in DNA. Note that the $\approx$100-ps anisotropy

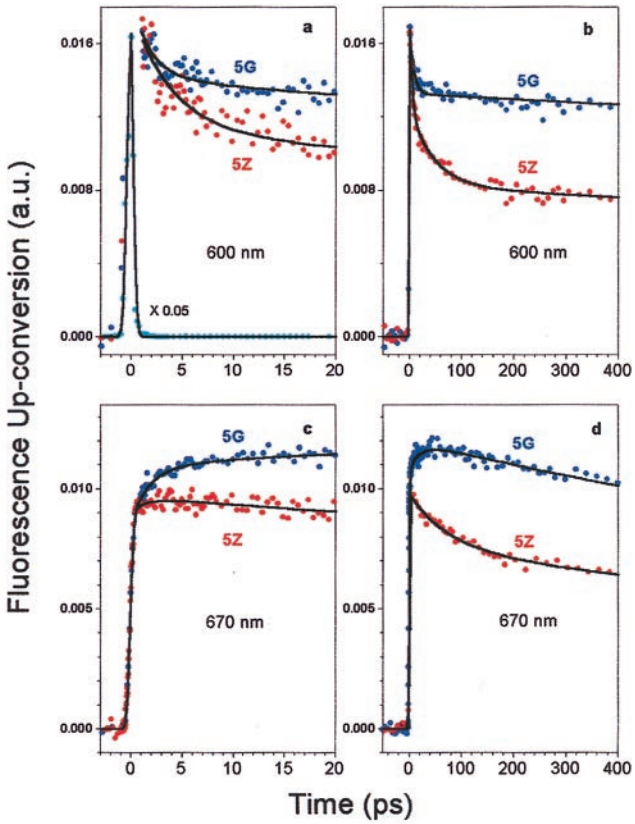

FIG. 3. Femtosecond fluorescence up-conversion of DNA assemblies with 5Z and 5G, detected at 600 nm (*Upper*) and 670 nm (*Lower*) in the short (*Left*) and the long (*Right*) time range. At the short wavelength, there is a solvent-alone spike around $t = 0$ (see *a*), which is absent at the longer wavelength (670 nm). The sample conditions are given in Fig. 2.

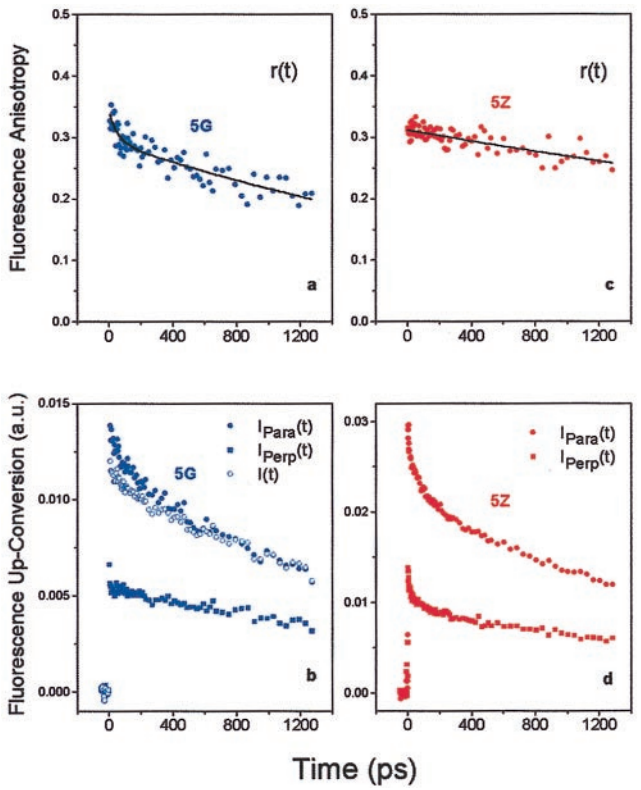

FIG. 4. Polarization dependence of the time-resolved fluorescence. The decays of the fluorescence anisotropy for 5G (*a*) and 5Z (*c*) are shown. Fluorescence decays $I_{\|}$ and $I_{\perp}$ (polarization of the detection with respect to the excitation) for 5G and 5Z are also given (*b* and *d*). The magic angle (54.7°) $I(t)$, deduced from $I_{\|}$ and $I_{\perp}$ for 5G (see *ET Dynamics*), is shown for comparison with $I_{\|}$. The sample conditions are given in Fig. 2.

decay component appears also in the parallel fluorescence signal $I_{\|}(t)$ shown in Fig. 4*b*. $I(t)$ is calculated in the following way: $I(t) = I_{\|}(t) + 2I_{\perp}(t)$, normalized to $I_{\|}(t)$ at longer times. It is equivalent to the signal at the magic angle (54.7°). Comparing $I(t)$ and $I_{\|}(t)$, it becomes evident that the latter contains an additional decay component of ≈100 ps caused by an orientational motion.

There are two types of trajectories with E having different geometries (orientations), one being initially *favorable* and the other initially *unfavorable* for ET. In reality, there is a whole distribution of orientations, but the ET emphasizes two families; those poised and those requiring time to dynamically switch on. Hence, the orientational motion within the DNA duplex is important for ET. We conclude that the 5-ps decay reflects the ET dynamics in those structures where E is "perfectly stacked," whereas the slow quenching process (75 ps) is caused by the fraction of molecules where E has to reorient/rotate first before ET can occur. The reason for the absence of the ≈100-ps anisotropy decay in 5Z is that the faster rotating molecules are immediately drained away by the ET process once they convert into the favorable geometry of ET. The 2-ns component represents those molecules that do not align favorably for ET.

Distance Dependence

An important question is how ET depends on the D–A distance. This dependence was examined by varying the position of Z within the 14-mer duplex while keeping the tethered E position constant. Both fluorescence up-conversion and transient absorption experiments reveal similar behavior, and we show only the transient absorption of 5Z, 6Z, and 7Z with a D–A separation of at least 10 Å, 14 Å, and 17 Å, respectively, and in reference to 5G, 6G, and 7G (Fig. 2). Clearly, the Z assemblies show unusual distance dependencies in their dynamical times and amplitudes. The G assemblies show essentially no variations within our experimental error; all transient absorption measurements of 5G, 6G, and 7G are similar in both the short and the long time scans and show ≈1.5-ps and ≈2-ns decays (Fig. 2, curve G).

In contrast, the transient absorption data of 5Z, 6Z, and 7Z indicate that ET occurs essentially with the same characteristic time constants for all distances studied but with a decreasing amplitude as the distance increases (Fig. 2, curve Z). In the order of 5Z, 6Z, and 7Z, the fast component (5 ± 1 ps) has the amplitude of 34%, 24%, and 14%. The slower component (75 ± 20 ps for 5Z and 6Z; 103 ± 34 ps for 7Z) has the amplitude of 23%, 22%, and 9%. Consequently, the total ET efficiency (5-ps and 75-ps decays) of the 5Z, 6Z, and 7Z are 57%, 46%, and 23%, respectively; here the efficiency is defined as the intensity drop in the ET decay normalized to the initial intensity. These efficiencies should be compared with the steady-state measurements: 70%, 56%, 28% for 5Z, 6Z, and 7Z, respectively, calibrated to the steady-state intensities of 5G, 6G, and 7G (18).

Mechanism: Transport and Molecular Motions

The striking observations reported here elucidate the elementary mechanism of DNA-mediated ET: independent of the D–B–A distance (10–17 Å), the rates are similar, whereas the ET efficiency decreases with increasing distance over the same

range. We consider first the determinants of the ultrafast time scale for ET and then the basis for variations in ET efficiency.

There are two fundamental concepts governing the ET process, the energetics of the D–B–A system and the time scale of the molecular motions during the transfer. The energetics play an important role in defining two extreme limits, that of *transport* through the B by multiple-step hopping and the other that involves a one-step *transfer* between D and A. The literature is rich in the application of these two extreme cases for one-dimensional excitation transfer in solids (ref. 41 and references therein), in molecular assemblies (42) and electronics (43), for ET in biological systems (44), and for many D–A systems (45). These issues of debating the role of chemical and physical transfer in bridged systems and the relative importance of thermodynamic and kinetic effects have roots in many studies of ET reactions in solutions (46, 47).

If the transfer is a one-step process, then the distance dependence of the rates is dramatic and can be described by the parameter β in a superexchange mechanism (48). In this case, there is an effective coupling between D and A that depends exponentially on the length of B. On the other hand, a transport process involves a real population residence in B, resulting in a weak distance dependence. Here the electronic coupling (V) is critical between D and B, within B, and between B and A. This picture is incomplete, however, as one must consider also the time scale for the orientational motion relative to that of ET in order for the transfer or transport to be effective. Achieving orientational coherence could in fact become the rate-determining step for ET (34).

In the system described here, with the initial femtosecond excitation of E, which is a cation in the ground state, an electron is promoted from the highest occupied molecular orbital to the lowest unoccupied molecular orbital (HOMO and LUMO, respectively) of E creating an electron-hole localized on E, the electron acceptor (hole donor). The interaction of $E^{+}*$ with the DNA B leads to a hole injection from $E^{+}*$ to B or more accurately from $E^{+}*$–B–Z to $E^{\bullet}$–$B^{\bullet+}$–Z. Because of the net driving force ($\Delta G \approx -0.2$ eV), there is a final "trapping" step which produces $E^{\bullet}$–B–$Z^{\bullet+}$. The energies of the three configurations are determining factors for the transport. Significantly, the overall transport is controlled by the rate of electron injection, governed by the electronic coupling V_{E-B}; the transport in the B, determined by V_{B-B}; and the trapping rate, governed by V_{B-Z}. Implicit in these rates is their dependence on the energetics of the base pairs and on the stacking of E, B, and Z.

We may estimate the time scale of ET between the $E^{+}*$–B–Z and $E^{\bullet}$–$B^{\bullet+}$–Z configurations by using the semiclassical Marcus expression (49). We assume that pulse radiolysis (50) and electrochemical (51) studies on the oxidation of the nucleotides and reduction of E (18) provide reasonable estimates of their values within DNA so that $\Delta G_{E,B} = 0.1$ eV and $\Delta G_{B,Z} = -0.3$ eV. Then if λ, the reorganization energy, is 0.1 eV and the electronic coupling matrix elements, V_{E-B} and V_{B-Z}, are 200 cm^{-1} at room temperature, we estimate k^{-1} for the first and the final steps to be $\approx$2 ps; changing λ from 0.1 eV to 0.2 eV changes the value of k^{-1} for the first step to $\approx$4 ps. The similarity of this value to the observed time scale for ET may suggest the adequacy of the parameters estimated for the transport, with the indication that the transfer in B is faster than that of the initial and/or final step. In fact, we observe no significant change in the rates with distance, and thus ET involves a rate-determining step that is independent of the steps in B.

We have carried out preliminary quantum calculations by using the ZINDO method (52, 53) and found that the coupling matrix elements range from 100 cm^{-1} to 400 cm^{-1} for adjacent base pairs and that the energy difference between E, Z, and the intervening B states, or the energy spread, is on the order of 0.3 eV. Thus we estimate $\approx$300 fs per step in the B for near resonance transport. There is no one defined energy difference to consider, because the energy spread is comparable to that of ΔG. It is important to realize that the effective coupling to B is sequence dependent, and we believe that the entire sequence should be considered collectively in calculating ΔG. Thus, ΔG for hole injection from E* to adenine will be smaller in EAAAG than in EATTG. The λ value given above is lower than those reported for ET in polar solvents (54) and in some proteins [refs. 31 (and references therein), 32, and 33], but it is comparable to those found for ET in less polar solvents (54) and in the photosynthetic reaction center (55); in DNA, the proximity of D and A to the B and the intercalation provides a unique environment that influences the value of λ. It should be noted that, in our systems, the transfer is not accompanied by (+−) charge separation; only carrier (+) transport is involved.

What about the efficiency of the transport? It is apparent that the structural dynamics of the DNA double helix must come into play. The ultimate yield of the transport depends on the spatial orientation of D, A, and the B base pairs—stacking—which dictates the magnitude of the effective coupling. As the dynamical nature of the DNA base stack gives rise to a distribution of conformations, only a fraction of the population is active for ultrafast ET. This distribution of local conformations will vary with DNA sequence (56). Moreover, all these conformations vary with time as a result of the dynamical motions within DNA, which occur on picosecond to millisecond time scales (57). In the DNA assemblies, the favorable and nonfavorable conformations give rise to the observed rates of ET, as discussed above. For DNA duplexes that contain certain defects (e.g., transiently destacked base pairs or reactants), coupling is reduced to such an extent that ET becomes impossible during the lifetime of the excited E. These inactive structures will contribute to the long ($\approx$2-ns) decay that we observe in both fluorescence and transient absorption experiments. As we do not observe a significant change in the three decay rates (5 ps, 75 ps, and $\approx$2 ns) with distance, the dynamical defect motions important here occur primarily on a time scale slower than the lifetime of E.

Accordingly, the observed dependence of the efficiency (yield) on distance is controlled by the "static" (on the time scale of the lifetime of E) distribution of ground-state conformations. Statistically, over longer distances, there will be a higher probability of defects in stacking, which explains our observed reduction in the amplitudes of both the 5-ps and the 75-ps components as we increase the distance from 5Z to 7Z. This decrease in yield is expected to depend exponentially on distance, but in duplexes with finite length, the dependence could deviate somewhat; the total ET efficiency changes in the order of 5Z, 6Z, and 7Z from 57% to 46% and to 23%. As such, these yield results will give a β value that does not reflect the actual behavior of the rates vs. distance; the yield reflects only the degree of disorder in the stacking. Finally, we expect that the coherence length of the B transport is on the order of the next-neighbor base-pair distances, because a coupling matrix element, V_{B-B}, of $\approx$200 cm^{-1} is comparable to kT at room temperature (T).

In conclusion, these results elucidate the elementary mechanism for carrier transport in DNA. The dynamics of this biological ET in D–B–A assemblies are governed by the local effective interactions of D (A) with the intervening base pairs and by the time scale of molecular motions. In the systems reported, where D and A are at a fixed distance apart, the ultrafast efficient ET becomes inefficient by 17 Å of separation, indicating the increased role of stacking disorder among members of the B. The use of the parameter β must be handled with care, as it is valid only if the energetics allow for a virtual coupling of D and A to the B. β may be used as a "figure of merit," but the physics must be clear regarding the mechanism of the transfer or transport.

This work would have not been possible without the support of the Laboratory for Molecular Sciences. T.F. is grateful for financial support from the Deutsche Forschungsgemeinschaft.

1. Eley, D. D. & Spivey, D. I. (1962) *Faraday Soc. Trans.* **58,** 411–415.
2. Hoffmann, T. A. & Ladik, J. (1964) *Adv. Chem. Phys.* **7,** 84–158.
3. Okata, Y., Kobayashi, T., Tanaka, K. & Shimomura, M. (1998) *J. Am. Chem. Soc.* **120,** 6165–6166.
4. Snart, R. S. (1968) *Biopolymers* **6,** 293–297.
5. Burrows, C. J. & Muller, J. G. (1998) *Chem. Rev.* **98,** 1109–1151.
6. Cadet, J. (1994) in *DNA Adducts: Identification and Significance*, eds. Hemminki, K., Dipple, A., Shiker, D. E. F, Kadlubar, F. F., Segerback, D. & Bartsch, H. (IARC, Lyon, France).
7. Baguley, B. C. & Lebret, M. (1984) *Biochemistry* **23,** 937–943.
8. Fromherz, P. & Rieger, B. (1986) *J. Am. Chem. Soc.* **108,** 5361–5362.
9. Barton, J. K., Kumar, C. V. & Turro, N. J. (1986) *J. Am. Chem. Soc.* **108,** 6391–6393.
10. Brun, A. M. & Harriman, A. (1992) *J. Am. Chem. Soc.* **114,** 3656–3660.
11. Arkin, M. R., Stemp, E. D. A., Holmlin, R. E., Barton, J. K., Hörmann, A., Olson, E. J. C. & Barbara, P. F. (1996) *Science* **273,** 475–480.
12. Lincoln, P., Tuite, E. & Norden, B. (1997) *J. Am. Chem. Soc.* **119,** 1454–1455.
13. Murphy, C. J., Arkin, M. R., Jenkins, Y., Ghatlia, N. D., Bossmann, S. H., Turro, N. J. & Barton, J. K. (1993) *Science* **262,** 1025–1029.
14. Meade, T. J. & Kayyem, J. F. (1995) *Angew. Chem. Int. Ed. Engl.* **34,** 352–354.
15. Lewis, F. D., Wu, T., Zhang, Y., Letsinger, R. L., Greenfield, S. R. & Wasielewski, M. R. (1997) *Science* **277,** 673–676.
16. Kelley, S. O., Holmlin, R. E., Stemp, E. D. A. & Barton, J. K. (1997) *J. Am. Chem. Soc.* **119,** 9861–9870.
17. Meggers, E., Michel-Beyerle, M. E. & Giese, B. (1998) *J. Am. Chem. Soc.* **120,** 12950–12955.
18. Kelley, S. O. & Barton, J. K. (1998) *Chem. Biol.* **5,** 413–425.
19. Fukui, K. & Tanaka, K. (1998) *Angew. Chem. Int. Ed. Engl.* **37,** 158–161.
20. Kelley, S. O. & Barton, J. K. (1999) *Science* **283,** 375–381.
21. Priyadarshy, S., Risser, S. M. & Beratan, D. N. (1996) *J. Phys. Chem.* **100,** 17678–17682.
22. Felts, A. K., Pollard, W. T. & Friesner, R. A. (1995) *J. Phys. Chem.* **99,** 2929–2940.
23. Okada, A., Chernyak, V. & Mukamel S. (1998) *J. Phys. Chem.* **102,** 1241–1251.
24. Jortner, J., Bixon, M., Langenbacher, T. & Michel-Beyerle, M. E. (1998) *Proc. Natl. Acad. Sci USA* **95,** 12759–12765.
25. Netzel, T. L. (1998) in *Organic and Inorganic Photochemistry*, eds. Ramamurthy, V. & Schanze, K. S. (Dekker, New York), pp. 1–54.
26. Ratner, M. (1999) *Nature (London)* **397,** 480–481.
27. Dandliker, P. J., Holmlin, R. E. & Barton, J. K. (1997) *Science* **275,** 1465–1468.
28. Hall, D. B., Holmlin, R. E. & Barton, J. K. (1996) *Nature (London)* **382,** 731–735.
29. Gasper, S. M. & Schuster, G. B. (1997) *J. Am. Chem. Soc.* **119,** 12762–12771.
30. Bixon, M. & Jortner, J., eds. (1998) *Adv. Chem. Phys.* **106**, 1–707.
31. Gray, H. B. & Winkler, J. R. (1996) *Annu. Rev. Biochem.* **65,** 537–561.
32. Moser, C. C., Keske, J. M., Warmcke, K., Farid, R. S. & Dutton, P. L. (1992) *Science* **355,** 796–802.
33. Evenson, J. W. & Karplus, M. (1993) *Science* **262,** 1247–1249.
34. Fiebig, T., Wan, C., Kelley, S. O., Barton, J. K. & Zewail, A. H. (1999) *Proc. Natl. Acad. Sci. USA* **96,** 1187–1192.
35. Hall, D. B., Kelley, S. O. & Barton, J. K. (1998) *Biochemistry* **37,** 15933–15940.
36. Olmsted, J., III, & Kearns, D. R. (1977) *Biochemistry* **16,** 3647–3654.
37. Millar, D. P., Robbins, R. J. & Zewail, A. H. (1980) *Proc. Natl. Acad. Sci. USA* **77,** 5593–5597.
38. Sommer, J. H., Nordlund, T. M., McGuire, M. & McLendon, G. (1986) *J. Phys. Chem.* **90,** 5173–5178.
39. Nordlund, T. M., Andersson, L. N., Rigler, R., Gräslund, A. & McLaughlin, L. W. (1989) *Biochemistry* **28,** 9095–9103.
40. Millar, D. P., Robbins, R. J. & Zewail, A. H. (1982) *J. Chem. Phys.* **76,** 2080–2094.
41. Smith, D. D., Millar, D. P. & Zewail, A. H. (1980) *J. Chem. Phys.* **72,** 1187–1208.
42. Larsson, S. (1982) *Faraday Discuss. Chem. Soc.* **74,** 390.
43. Aviram, A. & Ratner, M. A., eds. (1998) *Molecular Electronics: Science and Technology*, (N. Y. Acad. Sci., New York).
44. Clarke, M. J, Goodenough, J. B., Ibers, J. A., Jørgensen, C. K., Mingos, D. M. P., Neilands, J. B., Palmer, G. A., Reinen, D., Sadler, P. J., Weiss, R., *et al*., eds. (1991) *Long-Range Electron Transfer in Biology*, Structure and Bonding 75 (Springer, Berlin).
45. Meyer, J. T. & Newton, M. D. (1993) *Chem. Phys.* **176,** 289–649.
46. Taube, H. (1984) *Angew. Chem. Int. Ed. Engl.* **23,** 329–339.
47. Isied, S., ed. (1997) *Electron Transfer Reactions: Inorganic, Organometallic and Biological Applications*, Advances in Chemistry Series (Am. Chem. Soc., Washington, DC).
48. McConnell, H. M. (1961) *J. Chem. Phys.* **35,** 508–515.
49. Marcus, R. A. & Sutin, N. (1985) *Biochim. Biophys. Acta* **811,** 265–322.
50. Steenken, S. & Jovanivic, S. V. (1997) *J. Am. Chem. Soc.* **119,** 617–618.
51. Seidel, C. A. M., Schulz, A. & Sauer, M. H. M. (1996) *J. Phys. Chem.* **100,** 5541–5553.
52. Ridley, J. & Zerner, M. (1973) *Theor. Chim. Acta* **32,** 111–134.
53. Batlelle Pacific Northwest Laboratories (1992) ARGUS (Molecular Science Research Center, Richland, WA), Version 1.2.
54. Gould, I. R., Noukakis, D., Gomez-Jahn, L., Young, R. H., Goodman, J. L. & Farid, S. (1993) *Chem. Phys.* **176,** 439–456.
55. Bixon, M., Jortner, J. & Michel-Beyerle, M. E. (1995) *Chem. Phys.* **197,** 389–404.
56. Saenger, W. (1984) *Principles of Nucleic Acid Structure* (Springer, New York).
57. Robinson, B. H., Mailer, C. & Drobny G. (1997) *Annu. Rev. Biophys. Biomol. Struct.* **26,** 629–658.